1996ApJ...472L..130

THE ASTROPHYSICAL JOURNAL, 472:L13–L16, 1996 November 20
© 1996. The American Astronomical Society. All rights reserved. Printed in U.S.A.

AUTOMATED MORPHOLOGICAL CLASSIFICATION IN DEEP *HUBBLE SPACE TELESCOPE UBVI* FIELDS: RAPIDLY AND PASSIVELY EVOLVING FAINT GALAXY POPULATIONS[1]

STEPHEN C. ODEWAHN AND ROGIER A. WINDHORST
Department of Physics and Astronomy, Arizona State University, Box 871504, Tempe, AZ 85287-1504; sco@starburst.la.asu.edu, raw@starburst.la.asu.edu
SIMON P. DRIVER
School of Physics, University of New South Wales, Sydney, NSW 2052, Australia; spd@newt.phys.unsw.edu.au
AND
WILLIAM C. KEEL
Department of Physics and Astronomy, University of Alabama, Box 870324, Tuscaloosa, AL 35487-0324; keel@bildad.astr.ua.edu
Received 1996 January 29; accepted 1996 August 29

ABSTRACT

We analyze deep *Hubble Space Telescope* Wide Field Planetary Camera 2 (WFPC2) images in U, B, V, I using artificial neural network (ANN) classifiers, which are based on galaxy surface brightness and light profile (but *not* on color nor on scale length, r_{hl}). The ANN distinguishes quite well between E/S0, Sabc, and Sd/Irr+M galaxies (M for merging systems) for $B_J \lesssim 27$ mag. We discuss effects from the cosmological surface brightness (SB) dimming and from the redshifted UV morphology on the classifications, and we correct for the latter. We present classifications in *UBVI* from (a) four independent human classifiers; (b) ANNs trained on V_{606} and I_{814} images; and (c) an ANN trained on images in the *rest-frame UBV* according to the expected redshift distribution as a function of B_J. For each of the three methods, we find that the fraction of galaxy types does not depend significantly on wavelength, and that they produce consistent counts as a function of type.

The median scale length at $B_J \simeq 27$ mag is $r_{hl} \simeq 0\farcs25$–$0\farcs3$ (1–2 kpc at $z \approx 1$–2). Early- and late-type galaxies are fairly well separated in *BVI* color-magnitude diagrams for $B \lesssim 27$ mag, with E/S0 galaxies being the reddest and Sd/Irr+M galaxies generally blue. We present the B-band galaxy counts for five WFPC2 fields as a function of morphological type for $B_J \lesssim 27$ mag. E/S0 galaxies are only marginally above the no-evolution predictions, and Sabc galaxies are at most 0.5 dex above the nonevolving models for $B_J \gtrsim 24$ mag. The faint blue galaxy counts in the B band are dominated by Sd/Irr+M galaxies and can be explained by a *moderately* steep local luminosity function (LF) undergoing strong luminosity evolution. We suggest that these faint *late-type* objects (24 mag $\lesssim B_J \lesssim$ 28 mag) are a combination of low-luminosity lower redshift dwarf galaxies, plus *compact* star-forming galaxies and merging systems at $z \simeq$ 1–3, possibly the building blocks of the luminous early-type galaxies seen today.

Subject headings: galaxies: elliptical and lenticular, cD — galaxies: evolution — galaxies: formation — galaxies: irregular — galaxies: spiral

1. INTRODUCTION

The majority of explanations for the faint blue galaxy (FBG) excess observed in deep ground-based images (e.g., Kron 1982; Broadhurst, Ellis, & Shanks 1988; Tyson 1988; Driver et al. 1994; Neuschaefer & Windhorst 1995, hereafter NW95) involve irregular/dwarf populations, or objects with M_B fainter than -17.0 mag (using $H_0 = 80$, $q_0 = 0.5$ throughout). The $\sim 0\farcs1$ FWHM resolution provided by the *Hubble Space Telescope* (*HST*) Wide Field Planetary Camera 2 (WFPC2) allows the determination of the subkiloparsec morphology of distant galaxies—and hence of the population fractions of different galaxy types—over a wide range of epochs. Driver et al. (1995a, hereafter D95a), Driver, Windhorst, & Griffiths (1995b, hereafter D95b), Glazebrook et al. (1995), and Cowie, Hu, & Songaila (1995) used WFPC2 to study the morphological properties of faint galaxies. D95a showed that the FBG counts for $I_{814} \lesssim 24.5$ mag are dominated by late-type/irregulars, and suggest that neither a steep local luminosity function (LF) nor strong evolution alone can explain the high observed counts. Abraham et al. (1996) used a two-parameter space to assign types for $I_{814} \lesssim 25$ and reached the same conclusion as D95a. In view of these *HST* results, the development of a rigorous morphological classification scheme is important to study galaxy formation and evolution in an unbiased manner. One promising approach maps multivariate information to morphological types using an artificial neural network (ANN; see Odewahn et al. 1992, hereafter O92; Storrie-Lombardi et al. 1992; Odewahn 1995, hereafter O95; Naim et al. 1995). We have applied this technique to five WFPC2 fields in B_{450} ($\simeq B_J$), since in B_J the galaxy counts are steepest and the FBG excess will be most pronounced. V_{606} and/or I_{814} images are analyzed also for color information. In § 2, we discuss the observations, reduction, and the development and testing of our ANN classifiers. In § 3, we discuss the magnitude-size and color-magnitude relations (Figs. 1 and 2 [Pls. L1 and L2]) and the galaxy counts as a function of type for $B_J \lesssim 27$ mag (Fig. 3 [Pl. L3]), and discuss our results.

2. OBSERVATIONS, REDUCTION, AND ANN CLASSIFICATIONS

2.1. *WFPC2 Observations*

In cycle 4–5, we imaged a single deep dithered WFPC2 field surrounding the weak radio galaxy 53W002 (hereafter W02) at $z = 2.39$. These deep images provided 5 σ point-source

[1] Based on observations with the NASA/ESA *Hubble Space Telescope* obtained at the Space Telescope Science Institute, which is operated by AURA, Inc., under NASA contract NAS 5-26555.

© American Astronomical Society • Provided by the NASA Astrophysics Data System

1996ApJ...472L..130

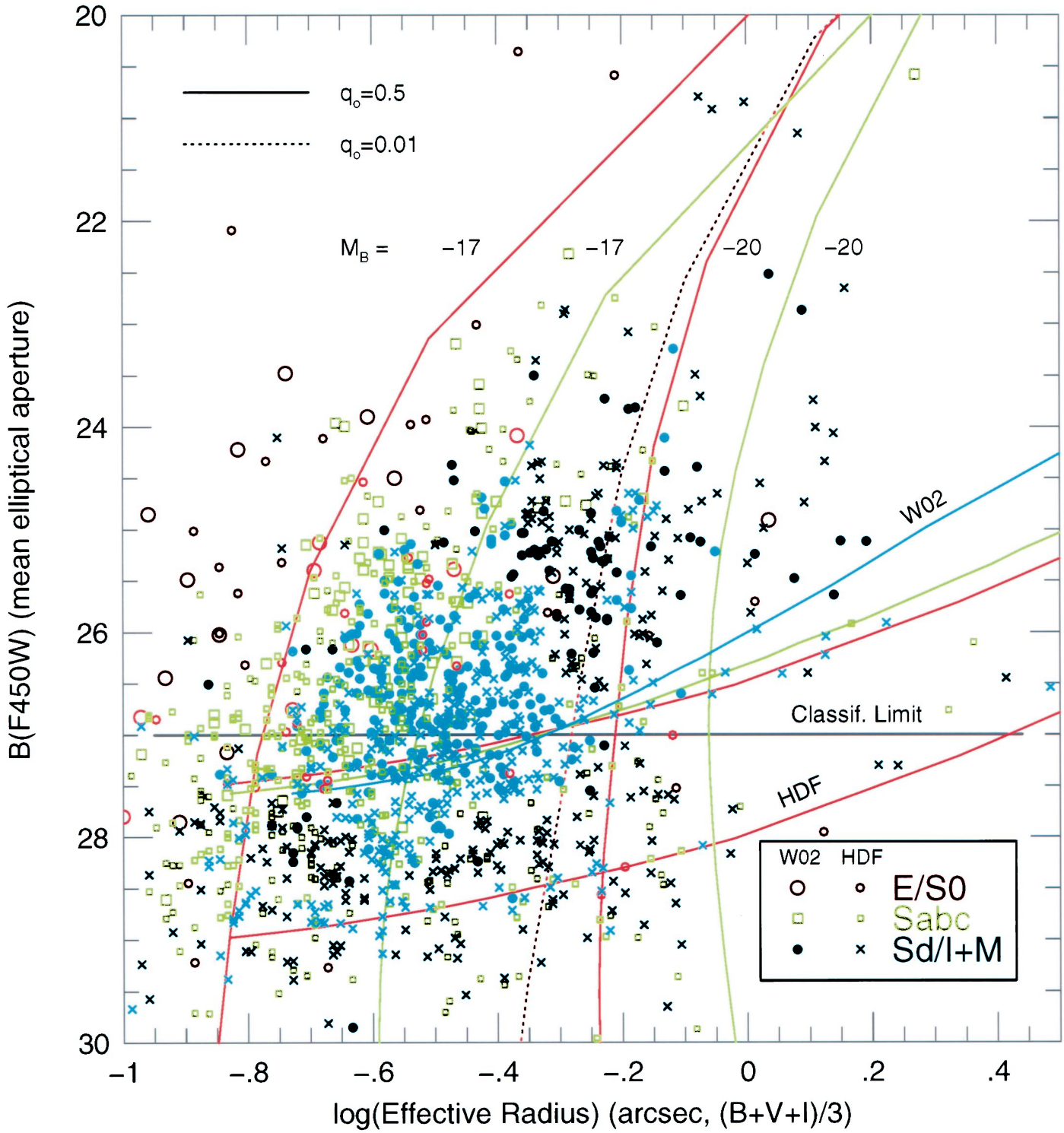

FIG. 1.—The B_{450} magnitude (aperture grown to total) vs. half-light radius r_{hl} (in arcseconds averaged over B_{450}, V_{606}, and/or I_{814}) for all classified galaxies in the 53W002 (W02) field and the Hubble Deep Field (HDF). Symbols indicate membership in the categories E/S0, Sabc, and Sd/Irr + M, as classified by the *rest-frame* ANN (see § 2.4). The solid almost-horizontal curves indicates the B_{450} detection limit for these two deep WFPC2 fields. The almost-vertical curves indicate how the median scale length of RC3 galaxies of given Hubble type and M_B decline toward fainter magnitude (see text). For $B_J \lesssim 27$ mag, where both samples are complete and the ANN is reliable, galaxies classified as E/S0 have on average smaller observed scale lengths than Sabc galaxies, which are smaller in general than Sd/Irr galaxies. The observed scale lengths reach a median of $r_{hl} \sim 0''.25$–$0''.3$ at $B_J \sim 27$ mag (~1.3 kpc for $H_0 = 80$, $q_0 = 0.5$, and the expected range $z \sim 0.5$–2.5).

ODEWAHN et al. (see 472, L13)

© American Astronomical Society • Provided by the NASA Astrophysics Data System

1996ApJ...472L..130

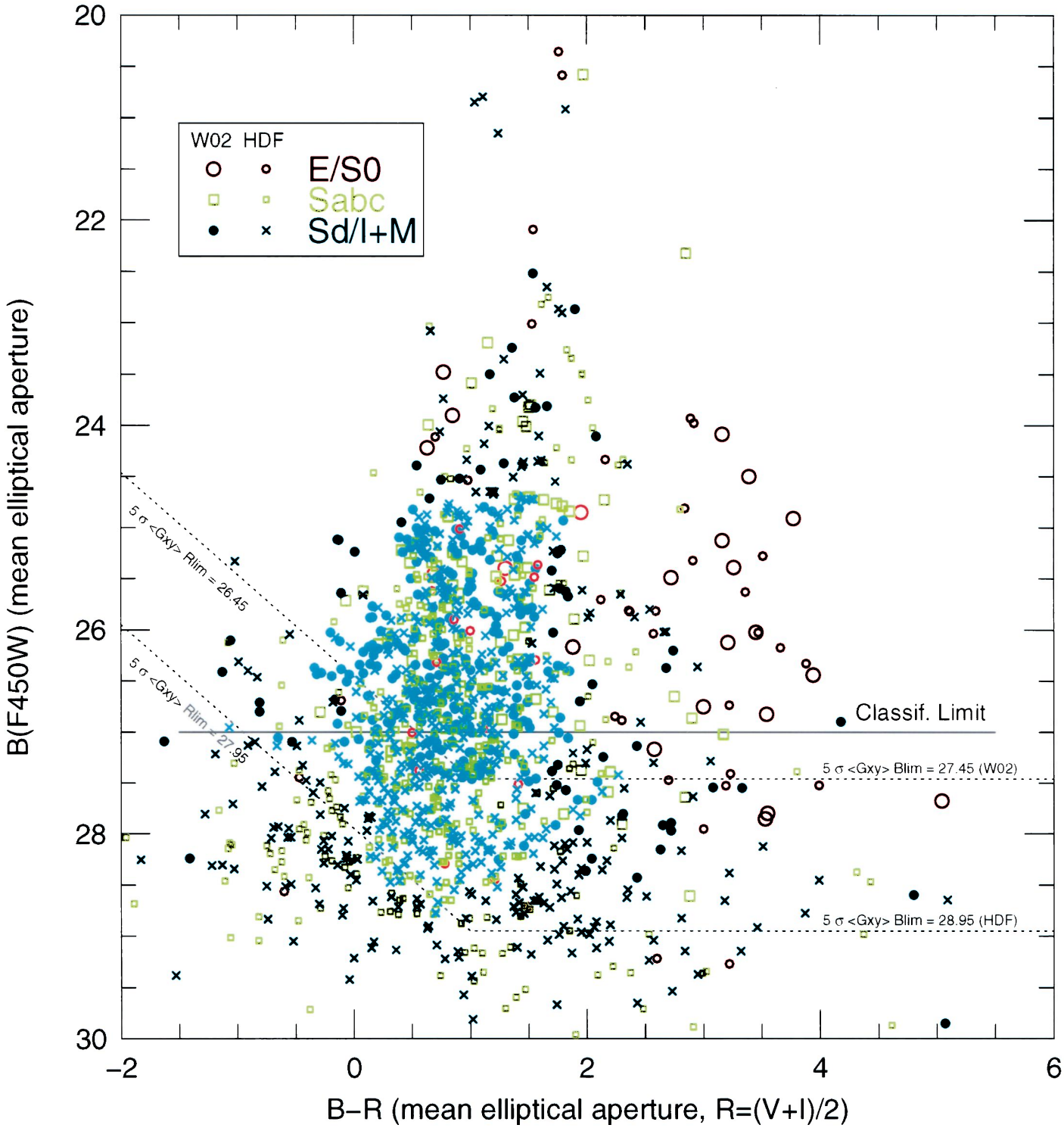

FIG. 2.—The $(B - R)$ vs. B_{450} color-magnitude diagram for all classified galaxies in the same deep WFPC2 fields as in Fig. 1. $(V_{606} + I_{814})/2$ was used as "wide R_{6900}" band to increase S/N in "$(B - R)$". The B_{450} image is substantially complete for galaxies of average SB at $B_J \lesssim 27.5$ mag (5 σ) in the W02 field and $B_J \lesssim 29.0$ mag in the HDF. For $B_J \gtrsim 26.0$ and 27.5 mag, the two fields become increasingly incomplete for the *bluest* objects due to the redder detection limits at $R \sim 26.5$ and 28.0 mag, respectively, as indicated by the two slanted dashed lines. The same ANN galaxy classes are indicated as in Fig. 1, which are reliable for $B_J \lesssim 27$ mag. The reddest objects at $B_J \lesssim 27$ mag are classified mostly as E/S0 and Sabc galaxies and do not increase as rapidly toward the formal completeness limits, suggesting that the formation of early-type galaxies may have been largely complete by $z \sim 1$ (see text). On the contrary, the increase of the late-type + merging population galaxies down to the detection and classification limit ($B_J \sim 27$ mag) is quite remarkable (see also Fig. 3*d*).

© American Astronomical Society • Provided by the NASA Astrophysics Data System

1996ApJ...472L..130

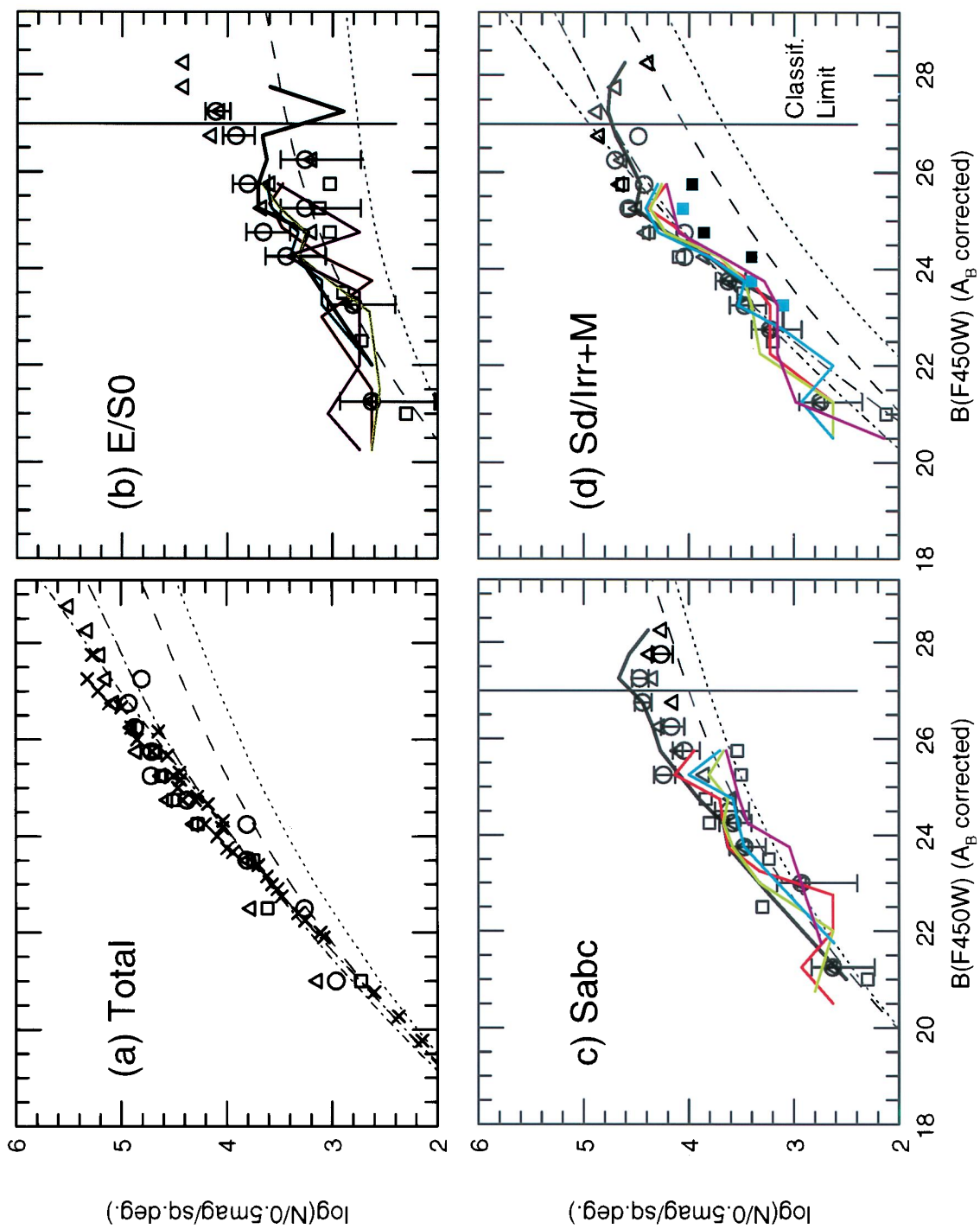

FIG. 3.—(*a*) Differential B_J band number counts from the W02 field (*open circles*), the HDF (*open triangles*), and three shallower WFPC2 B_{450} fields (*open squares*), as well as previous ground-based B_J band counts (*crosses*). Error bars are shown only when larger than the symbol size, and only for the W02 counts (errors are similar for the other fields). Panels show (*a*) all galaxies, (*b*) *HST* ellipticals (E/S0 galaxies), (*c*) early-type spirals (Sabc galaxies), and (*d*) Sd/Irr+M galaxies. B_J number counts from *eyeball* classifications by four independent classifiers are shown as solid color-coded curves for the combined samples classified in U_{300} (*purple*), B_{450} (*blue*), V_{606} (*green*), and I_{814} (*red*). Heavy black curves in (*b–d*) indicate types from the *rest-frame* ANN classifiers (see text). Data points in (*b–d*) indicate the *single-band* ANN types from the five WFPC2 fields surveyed. All models are plotted as thin curves. The best-fit nonevolving models in (*b–d*) are based on the local LFs of Marzke et al. (1994; *long-dashed curve*) and Loveday et al. (1992; *dotted curve*). The E/S0 and Sabc populations show little evolution for $B_J \lesssim 26$ mag ($z \lesssim 1$); the excess with respect to the nonevolving Marzke case is $\lesssim$0.3–0.5 dex. Panel (*d*) shows model fits for an *evolving* Sd/Irr+M population (starburst with ΔLum = 1.5 mag at $z \approx 0.5$ and a local Marzke LF [*long-dash–dotted line*]) and a *nonevolving* dwarf-rich population (steep LF with $\alpha = -2.0$ [*short-dash–dotted line*]). Panel (*a*) shows the sum of the three best models from (*b–d*) and counts *all* detected objects. The late-type galaxy population in panel (*d*) must have evolved strongly and/or be dwarf dominated, and it causes most of the faint blue galaxy excess.

© American Astronomical Society • Provided by the NASA Astrophysics Data System

1996ApJ...472L..130

detection for B_{450}, $V_{606} \lesssim 28.4$ and $I_{814} \lesssim 27.6$ mag and a 1 σ surface brightness (SB) sensitivity for B, $V \lesssim 27.5$ and $I \lesssim 26.7$ mag arcsec^{-2} (for details, see Windhorst & Keel 1996, hereafter WK96; D95a). We compare our W02 galaxy counts to those from *UBVI* images in the Hubble deep field (HDF; Williams et al. 1996), which reach ~0.8–1.2 mag deeper (see § 3). Three shallower WFPC2 B_{450} and I_{814} fields (Schade et al. 1995) from the *HST* archive were included for $B \lesssim 25.5$ mag to obtain better statistics at the bright end.

2.2. *Data Processing and Catalog Generation*

All images in each filter were registered spatially and averaged to create high signal-to-noise ratio (S/N) composites (see WK96), from which object catalogs were computed (see D95a, D95b). Potential objects were located and measured using aperture magnitudes grown to total (see D95a; D95b; Pascarelle et al. 1996a, 1996b [hereafter P96a, P96b]). Compared to the interactive package of P96a, we produce sky estimates consistent within 0.07% and aperture magnitudes grown to total consistent within 0.05 mag (with an rms ≃ 0.22 mag for each algorithm). These (*U*)*BVI* catalogs were used to produce a final catalog by selecting any object present in *any* filter with S/N ≥ 3. Hence, we do not exclude very red or very blue objects. Surface photometry was carried out with the automated image analysis package MORPHO (Odewahn 1995), giving ellipse fits over a range of isophotal levels, elliptically averaged SB profiles, and a set of type-dependent photometric parameters (see Odewahn & Aldering 1995, hereafter OA95; and § 2.3 below).

2.3. *ANN Classifications*

We assigned a morphological type to each galaxy in several independent ways. First, we classified by eye 173 galaxies with $U_{300} \lesssim 26$ mag, 372 in B_{450} (≲26.5 mag), and 542 in V_{606} and I_{814} (≲26 mag), including 173 galaxies in V and I from D95b ($I_{814} \lesssim 22$ mag), and obtained results mutually consistent within ±2 (rms) Hubble classes and scale errors ≲10% on the 16 step Hubble scale. Second, we classified all objects with $B_{450} \leq 27.5$ mag using ANN analysis of photometric parameters (O92, O95). ANNs are systems of weight vectors, whose component values are established through an iterative learning algorithm such as back-propagation (Rumelhardt & McClelland 1988). They take as input a linear set of patterns and produce as output a numerical pattern encoding an object classification. O95 shows that this pattern can be used to assign a confidence value to the estimated type. For this work, we adopt a type based on the mean nodal output of the ANN (error estimates for ANN types will be presented in Odewahn & Windhorst 1997). Fundamental to the development of such pattern classifiers is the existence of a large sample of examples (or "training set").

We developed a set of ANN classifiers for the I_{814} and V_{606} images using the morphological I_{814} eyeball classifications as a training set, as described above (see also D95b). To increase the number of training cases compared to our previous I_{814} studies, all four authors classified visually the D95b, W02, and HDF images in all available filters using the revised Hubble classification system. Each classifier inspected *both* the digital image *and* the SB profile for each galaxy in each filter. Hence, some profile information was incorporated in these eyeball estimates. These type estimates allowed us to (i) increase significantly our sample size for ANN training and testing, (ii) determine the repeatability of visual type estimates, and (iii) investigate systematic effects of the differential *K*-corrections (redshifted UV morphology) on our type estimates.

Following Odewahn & de Vaucouleurs (1992), we compared our morphological type catalogs in U, B, V, I to assess systematic effects introduced by classifier and filter. A few personal systematics between the four human classifiers were removed using small linear corrections. Types from the different classifiers vary in scale at the ≲10% level with a combined (rms) scatter of ≲2.0–2.5 type steps. The 1 σ error attached to a single classification is thus ±2.0 steps for $B_{450} \leq 25$ mag. These catalogs show good agreement with the I_{814} catalogs of D95a and D95b. Remarkably, we see little evidence of systematic biases in the type estimates due to the filter used (see § 2.4 and Fig. 3). The B versus I comparison in the W02 and HDF samples, and even the U versus I type comparison from the HDF sample, produce only slope variations of 5%–15% (at the ≲2 σ level) in the sense that galaxies were classed systematically *later* in the bluer bandpass. With the mean visual types from our W02 + HDF + D95b samples in U, B, V, or I, we developed ANN galaxy classifiers using six primary parameters: the SB at the 25% and 75% quartile radii, the mean SB within the effective radius and within an isophotal radius, as well as the slope and intercept of a linear fit to the SB profile (in $r^{1/4}$ space). These ANNs are based on the observed galaxy SB profile, but *not* on color, *nor* on scale length. Although trained on *different* 70% subsets of the existing catalogs, a direct comparison of the types provided by the V_{606} and I_{814} band classifiers (for $I_{814} \leq 24$ mag) produced a scale difference of ≲5% and a scatter of ≲1.7 type steps (rms). We developed also ANN classifiers designed to type galaxies in their appropriate *rest-frame UBV* filters. These rest-frame ANNs are described in detail in § 2.4 and produced types that were in remarkably good agreement with the visually derived types, as well as with the *single-filter* ANN types (see Fig. 3).

2.4. *Tests of Our Classification Systems as Function of Wavelength and Redshift*

Since for faint galaxies ($B_J \gtrsim 24$ mag) the expected median redshift is $z \gtrsim 0.7$ (Koo & Kron 1992), the B_{450} filter could look back into the rest-frame mid-UV. At higher redshifts (and fainter fluxes), V_{606} and even I_{814} may have the same problem. Therefore, we are concerned with how the cosmological $(1 + z)^4$ SB dimming and the wavelength dependence of the rest-frame (UV) morphology affect the ANN classifications. As discussed above, we observe little or *no* systematic change in the eyeball morphological types between the U, B, V, and I filters (see Fig. 3). This was the case even at the faintest levels ($B \sim 26$ mag) to which human classifications were made. This suggests that the properties on which our human classifiers rely (morphology and light profile) are more uniform with spectral bandpass than we would expect, or that the median redshift for the faint galaxy sample is somewhat smaller ($z \sim 1.0$ for $B_J \gtrsim 25$) and the redshift distribution wider than expected, so that cosmological effects possibly do not yet differ greatly between the B, V, and I filters.

To investigate this further, we designed a set of ANN classifiers that are valid for *rest-frame* filters. For this we used the following steps: (1) the likely redshift range was estimated for each B_{450} interval using the B_J redshift distributions of Koo & Kron (1992) and Ellis et al. (1996), and spectral evolution models for Gunn $g \lesssim 26$ mag from NW95; (2) using the known *UBVI* filter responses, these redshift ranges were used to estimate the most likely *rest-frame* central wavelength for each galaxy image; (3) then we selected a series of *rest-frame*

© American Astronomical Society • Provided by the NASA Astrophysics Data System

1996ApJ...472L..130

UBV images and derived the corresponding rest-frame ANNs. These produced good type segregation *with no obvious dependence on the original filter from which the image was drawn*. All *B*, *V*, and *I* images from our WFPC2 samples were classified this way using the most appropriate rest-frame classifier in *U*, *B*, and/or *V*. Independent estimates from different filters were averaged to produce a mean morphological type for each galaxy.

For galaxies with $B_{450} \leq 26$ mag, we compared these *rest-frame* ANN types to the *UBVI* eyeball classifications, as well as to the types predicted by the single-filter ANN classifiers. The *rest-frame* predictions for $B_J \lesssim 27$ do not differ significantly from the mean eyeball estimates, nor from the single-filter ANN estimates (see Fig. 3). The four-color counts in Figure 3 show *no* obvious evidence that the shorter wavelength filters result in a larger fraction of late-type galaxies. This is counterintuitive to the expectation that the redshifted UV continuum will tend to cause galaxies to be classified as later types. We believe that this is due to the fact that the elliptically averaged galaxy *profiles* that were used by the ANN are less wavelength dependent than the *morphology* (de Jong & van der Kruit 1994), in combination with a redshift distribution that becomes *wider* for *UBVI* $\gtrsim 25$ with a median that only increases slowly with redshift. In summary, we believe that for $B_J \lesssim 27$ mag both methods of ANN classification are reliable, but for $B_J \gtrsim 27$ significant discrepancies may exist between the I_{814} or V_{606} ANNs and the *rest-frame* ANNs (see Fig. 3), indicating that the median z may be $\gtrsim 2$ and that the uncertain far-UV morphology becomes important.

As a final check on systematic errors, we developed a faint galaxy simulation code to study the effects of decreasing S/N and image resolution on our ANN types. Using actual high-resolution, high-S/N images of large nearby galaxies as input, each image is repixelated to simulate the WFPC2 image at higher redshifts. Simulated images were processed in the same way as the WFPC2 samples. We found no strong trend for the predicted type to change significantly with redshift. There was a slight tendency to predict types that are *earlier* by one to two steps at higher z, but if real, this would serve only to weaken the result we report in § 3.3: a large fraction of faint late-type galaxies.

About 15% of all galaxies with $B_{450} \leq 25.5$ mag and classified by the ANN systems as late-type spirals or irregulars were classified as merging systems by the human classifiers. For $B_{450} > 25.5$ mag, the number of merging systems increases to 35% of those ANN-classified Sd/Irr galaxies. Hence, a good fraction of our ANN-classified "late-type" systems are actually merger morphologies, so we will designate this class as Sd/Irr + M systems.

3. WFPC2 B_{450} RESULTS AND DISCUSSION

3.1. *The Scale Length–Magnitude Relation*

Figure 1 shows the scale length r_{hl} (averaged over the *BVI* filters in which the object was detected to increase S/N) versus B_J magnitude for both the W02 and the HDF galaxies. The three main galaxy classes resulting from the *rest-frame* ANN are indicated with different colors, as are the formal 50% completeness limits for both fields computed for nearby RC3 galaxies of the same types. We plot also the best-fit models to the *local* r_{hl} versus M_B relations for RC3 mid-type spirals and ellipticals for a median $r_{hl} = 4.7$ and 3.2 kpc, respectively, assuming model redshift distributions (see Carlberg & Charlot 1992; NW95) and *K*-corrections (Bruzual & Charlot 1993; D95a; D95b) as a function of galaxy type (using $q_0 = 0.5$; but in one case also for $q_0 = 0.01$). The ANN distinguishes quite well between E/S0, Sabc, and Sd/Irr+M galaxies for $B_J \lesssim 27$ mag. In general, r_{hl} is smallest at a given flux for E/S0 galaxies. The median scale length at $B_J \simeq 27$ mag is $r_{hl} \simeq 0\farcs25$–$0\farcs3$, which corresponds to ~1.2–2.5 kpc for the redshift range $z \sim 0.5$–2.5 (and $q_0 = 0.01$–0.5). These values appear to be smaller than the characteristic scale lengths of mid- to late-type galaxies measured locally, as well as those measured with *HST* for $z \lesssim 0.8$ (or $B_J \lesssim 23$ mag; see Mutz et al. 1994). A possible explanation is that the faint galaxy population becomes progressively more dominated by lower luminosity and therefore smaller late-type objects at fainter fluxes (see Driver et al. 1994; D95b).

3.2. *The Color-Magnitude Diagram*

The total B_{450}-magnitude versus $(B - R)$ color is shown for each type in Figure 2, where we used "wide R" $\equiv (V + I)/2$ to increase S/N in colors. Figure 2 becomes increasingly incomplete at $B_J \gtrsim 26.0$ for the *bluest* W02 objects, because of the *red* detection limit at $R \simeq 26.5$ mag, as indicated by the slanted dashed lines (the HDF limits are again ~1.5 mag fainter). Only objects detected in all three filters are plotted here, but the fraction of objects seen only in B_{450} (at $B_J \lesssim 27$ mag) and not in V_{606} and/or I_{814}—as well as those seen only in V_{606} and I_{814} ($\lesssim$26 mag) and not in B_{450}—is $\lesssim$5%. Of significance is the clear segregation between the early- and the late-type galaxies for $B_J \lesssim 27$ mag, even though *no* color information was used by the ANN classifier. E/S0 galaxies are almost without exception the reddest galaxies at any flux level, and Sd/Irr+M galaxies are generally blue, at least down to the formal detection limit. Mid-type spirals (Sabc galaxies) have colors with large dispersion and about as blue as Sd/Irr galaxies, as expected from the (slightly) different colors measured for these populations locally (OA95) and the *K*-corrections for galaxies with ongoing star formation at $z \sim$ 1–2 (Bruzual & Charlot 1993). For $B_J \gtrsim 27$ mag, the galaxies in Figures 1 and 2 have larger classification errors—in addition to larger photometric errors and possibly larger cosmic scatter in the colors—although E/S0 galaxies are still generally redder and have smaller r_{hl}, while late types are generally bluer and have larger r_{hl}. Without further calibration in the rest-frame UV, we do not believe currently that the ANN classifier is reliable for $B_J \gtrsim 27$ mag (see also § 3.3), since a significant fraction of these objects may be at $z \gtrsim 2$. This is the major limiting factor in the ANN classes, and not the S/N of the faint objects, since the W02 and HDF samples yield consistent classes as a function of flux (see Fig. 3), yet have a S/N that differs by 1.2–1.5 mag at a given flux.

The increase in the relative fraction of late-type and merging galaxies (Sd/Irr+M) in Figure 3 toward fainter B_{450} is quite remarkable. They exist essentially down to the very detection limit, despite their larger relative scale lengths (Fig. 1). The redder objects—mostly classified as E/S0 galaxies—do not increase as rapidly toward the completeness limits ($B_J \lesssim 27$ mag) as the late types. Since early-type objects do not generally have the largest scale lengths (Fig. 1) nor the lowest SBs, this is probably not due to large differences in their redshift distribution—and therefore due to a larger cosmological SB dimming—but it may suggest that the formation of early-type galaxies was largely complete by the median redshift corresponding to $B \simeq 26$–27 mag (probably $z \gtrsim 1$; see NW95), so that their counts would indeed be converging for $B \gtrsim 26$ mag.

© American Astronomical Society • Provided by the NASA Astrophysics Data System

1996ApJ...472L..130

3.3. *The Galaxy Counts versus Type for $B_J \lesssim 27$ mag*

In Figure 3 we plot the differential B_J number counts for the different morphological types (E/S0, Sabc, Sd/Irr+M) in the five WFPC2 B_{450} fields. The plotted counts are based on mean types from our *visually* classified U, B, V, and I images (*color-coded lines*), from the $I_{814} + V_{606}$ *single-filter* ANN types (*data points*), and the *rest-frame* ANN types (*heavy unbroken lines*). Within the formal errors, Figures 3*a*–3*d* show that the total B_{450} counts in the W02 field are consistent with those in the three shallower B_{450} fields, as well as with ground-based counts (Metcalfe et al. 1995) and the deeper HDF counts down to their respective completeness limits, or $B_J \lesssim 27.0$ mag, whichever is brighter. Hence, field-to-field variations are no larger than the formal errors, and the ANN provides indeed consistent types given the S/N limitations.

Following D95a and D95b, we modeled the B_J number counts for the three main morphological types separately. Figure 3*b* shows that the B_J band counts of E/S0 galaxies follow the predictions for passively or mildly evolving models for $B_J \leq 24$ mag, and for $B_J \geq 24$ mag the observed counts are at most 0.3 dex higher than these models. Figure 3*c* shows that Sabc galaxies are consistent with these models for $B_J \leq 24$ mag and are at most 0.5 dex higher for 24 mag $\lesssim B_J \lesssim 27$ mag. Hence, a scenario invoking strong luminosity evolution is probably *not* required for the early-type galaxies out to $B_J \lesssim 27$ mag ($I_{814} \lesssim 25$ mag or $z \sim 1$), suggesting that their formation was largely complete by $z \sim 1$. We note that an epoch dependent merger rate [$\propto(1+z)^n$ with $n \gtrsim 2$; e.g., Burkey et al. 1994] could also explain a somewhat higher E/S0 and Sabc count for $B_J \geq 24$ mag. From a spectroscopic survey for $z \lesssim 1$, Lilly et al. (1995) deduce a similar lack of evolution for early-type galaxies as found here and in D95a. Our morphological studies can push this work now another 3 mag fainter than can be done spectroscopically.

Figure 3*d* shows that nonevolving models are clearly inadequate to explain our high WFPC2 B_J number counts for the Sd/Irr+M population. The fraction of visually classified merging systems is plotted as blue squares. The number of such systems rises strongly for $B_{450} \gtrsim 23$ mag, with up to one-third of our late-type systems possibly being mergers. For $B_{450} \gtrsim 22$ mag, the number counts of the *classical* Sd/Irr galaxies derived from both the ANN and visual type catalogs lie well above the nonevolving models. It is clear that the FBG excess is dominated by galaxies with late types, with a nonnegligible fraction of merging morphologies. The best-fit linear slope to the observed Sd/Irr+M counts for $24 \lesssim B_J \lesssim 28$ mag is 0.32 ± 0.04, similar to that of the total B_J counts (Fig. 3*a*).

Since spectroscopy of FBGs with $26 \lesssim B_J \lesssim 29$ mag may be impossible even for 8–10 m telescopes, we conclude this section by speculating briefly on the possible nature and evolution of these faint blue compact objects. Their small scale lengths (Fig. 1) suggest that a significant subset could be lower redshift ($z \sim 0.5$–1), lower luminosity objects (see D95b), in combination with some fraction of very compact ($r_{hl} = 1$–2 kpc) objects at $z \sim 1$–3. A nonevolving dwarf population fits the FBG counts quite well (Fig. 3*d*) but is inconsistent with the redshift distributions observed for $B_J \lesssim 24.5$ mag (see Phillipps & Driver 1995), and therefore it cannot be the only explanation. Consistent with the I_{814} band counts of D95a, our Sd/Irr+M B_{450} counts (Fig. 3*d*) can be described by a population with a *moderately* steep local LF (see Marzke et al. 1994; or steeper, with the high normalization of D95b), that underwent significant luminosity evolution since $z \lesssim 1$ (see Phillipps & Driver 1995). Alternatively, a starburst with $\Delta\mathrm{lum} \simeq 1.5$ mag at $z \simeq 0.5$–1 could explain the steep B_J counts for late types. Both models are shown in Figures 3*a* and 3*d*.

In such a scenario, a nonnegligible fraction of the FBGs with $25 \lesssim B_J \lesssim 29$ may be at $z \sim 1$–3. Cowie et al. (1995) found a good fraction of their faint *HST* galaxies at $z \gtrsim 1$, and Pascarelle et al. (1996a, 1996b) found 18 faint blue *compact* objects in the W02 field at $z = 2.39$ (through deep WFPC2 narrow-band redshifted Lyα imaging with five spectroscopic confirmations). A nonnegligible fraction of the FBG population could thus be similar compact, sub-galactic sized objects ($r_{hl} \lesssim 1$–2 kpc) in the range $z \simeq 1$–3.5 (see Fig. 1). Such objects may have been the reservoir of building blocks out of which the luminous early-type galaxies were formed through repeated merging, a process that must have been completed largely by $z \sim 1$ (Figs. 3*b*–3*c*), with some residual epoch-dependent merger rate (see Burkey et al. 1994). The fact that 20%–35% of our galaxies classified as late-type by the ANN appear to be merging systems, with that fraction increasing at fainter magnitudes, tends to support this possibility.

We thank Dave Burstein for helpful suggestions and acknowledge support from *HST* grants GO.5308.0.93A, GO.5985.0.94A, GO.2684.03.94A, and AR.6385.01.95A.

REFERENCES

Abraham, R., Tanvir, N. R., Santiago, B., Ellis, R. S., Glazebrook, K. G., & van den Bergh, S., 1996, MNRAS, 279, L47
Broadhurst, T. J., Ellis, R. S., & Shanks, T. 1988, MNRAS, 235, 827
Bruzual A. G., & Charlot S. 1993, ApJ, 405, 538
Burkey, J. M., Keel, W. C., Windhorst, R. A., & Franklin, B. E. 1994, ApJ, 429, L013
Carlberg, R. G., & Charlot, S. 1992, ApJ, 397, 5
Cowie, L. L., Hu, E. M., & Songaila, A. 1995, AJ, 110, 1576
de Jong, R. S., & van der Kruit, P. C. 1994, A&AS, 106, 451
Driver, S., Phillipps, S., Davies, J., Morgan, I., & Disney, M. 1994, MNRAS, 266, 155
Driver, S. P., Windhorst, R. A., Ostrander, E. J., Keel, W. C., Griffiths, R. E., & Ratnatunga, K. U. 1995a, ApJ, 449, L23 (D95a)
Driver, S. P., Windhorst, R. A., & Griffiths, R. E. 1995b, ApJ, 453, 48 (D95b)
Ellis, R. S., Colless, M., Broadhurst, T., Heyl, J., & Glazebrook, K. 1996, MNRAS, 280, 235
Glazebrook, K., Ellis, R. E., Santiago, B., & Griffiths, R. E. 1995, MNRAS, 275, L19
Koo, D. C., & Kron, R. G. 1992, ARA&A, 30, 613
Kron, R. G. 1982, Vistas Astron., 26, 37
Lilly, S. J., Tresse, L., Hammer, F., Crampton, D., & LeFevre, O. 1995, ApJ, 455, 108
Loveday, J., Peterson, B. A., Efstathiou, G., & Maddox, S. J. 1992, ApJ, 390, 338
Marzke, R. O., Geller, M. J., Huchra, J. P., & Corwin, H. G. 1994, AJ, 108, 437
Metcalfe, N., Shanks, T., Fong, R., & Roche, N. 1995, MNRAS, 273, 257
Mutz, S. B., et al. 1994, ApJ, 434, L055
Naim, A., Lahav, O., Sodre, L., & Storrie-Lombardi, M. C. 1995, MNRAS, 275, 567
Neuschaefer, L. W., & Windhorst, R. A. 1995a, ApJ, 439, 14 (NW95)
Odewahn, S. C. 1995, PASP, 107, 770 (O95)
Odewahn, S. C., & Aldering, G. 1995, AJ, 110, 2009 (OA95)
Odewahn, S. C., & de Vaucouleurs, G. 1992, ApJS, 83, 65
Odewahn, S. C., Stockwell, E. B., Pennington, R. M., Humphreys, R. M., & Zumach, W. A. 1992, AJ, 103, 318 (O92)
Odewahn, S. C., & Windhorst, R. A. 1997, in preparation
Pascarelle, S. M., Windhorst, R. A., Driver, S. P., Ostrander, E. J., & Keel, W. C. 1996a, ApJ, 456, L21
Pascarelle, S. M., Windhorst, R. A., Keel, W. C., & Odewahn, S. C. 1996b, Nature, 383, 45 (P96b)
Phillipps, S., & Driver, S. P. 1995, MNRAS, 274, 832
Rumelhardt, D. E., & McClelland, J. L. 1988, Explorations in Parallel Distributed Processing (Cambridge: MIT Press)
Schade, D., Lilly, S., Crampton, D., Hammer, F., LeFevre, O., & Tresse L. 1995, ApJ, 451, L1
Storrie-Lombardi, M. C., Lahav, O., Sodre, L. J., & Storrie-Lombardi, L. J. 1992, MNRAS, 258, 8
Tyson, J. A. 1988, AJ, 96, 1
Williams, R. E., et al. 1996, AJ, in press
Windhorst, R. A., & Keel, W. C. 1996, ApJ, submitted (WK96)

© American Astronomical Society • Provided by the NASA Astrophysics Data System